AIAA SciTech Forum
13-17 January 2014, National Harbor, Maryland
52nd Aerospace Sciences Meeting

10.2514/6.2014-1161

Large-Eddy Simulations of a Dual-Mode Scramjet Combustor: Operating Point "A" of University of Virginia's Scramjet Experiments

Wai Lee Chan*
University of Michigan, Department of Aerospace Engineering, Ann Arbor, MI, 48109, U.S.A.
Matthias Ihme†
Stanford University, Department of Mechanical Engineering, Stanford, CA, 94305, U.S.A.

Large-eddy simulations of the operating point "A" of the University of Virginia's dual-mode scramjet experiments are performed with the objective to evaluate the applicability of the flamelet/progress variable combustion model to compressible reacting flow environments. Results from this work will contribute to the ongoing efforts in advancing the incorporation of large-eddy simulation methodologies in the design of practical high-speed air-breathing propulsion systems. Reacting simulation results have shown qualitative agreements with previous numerical investigations and measurements for this operating point. Algorithmic development and modeling progress that enable the simulation of these flowfield environments are presented.

Nomenclature

t	Time, s
x	Position, m
ρ	Density, kg/m^3
u	Velocity, m/s
ω	Vorticity, 1/s
Z	Mixture-fraction
C	Progress variable
$\dot{\omega_C}$	Source term for progress variable, kg/(m$^3 \cdot$ s)
E	Total energy, including chemical energy, J/kg
h	Sensible and chemical enthalpy, J/kg
k	Turbulent kinetic energy, J/kg
p	Pressure, Pa
D	Diffusion coefficient, m^2/s
μ	Dynamic viscosity, Pa $\cdot$ s
ν	Kinematic viscosity, m^2/s
λ	Thermal conductivity, W/(m $\cdot$ K)
c_p	Specific heat capacity, J/(kg $\cdot$ K)
τ_{ij}	Viscous stress tensor, N/m^2
Sc	Schmidt number
Pr	Prandtl number
ϕ	General notation for conserved variables
$\mathcal{C}_\phi$	Turbulent model coefficient for scalar ϕ
Δ	Local filter width

*Graduate Student Research Assistant, Member AIAA.
†Assistant Professor, Member AIAA.

α_N	Nth criterion of shock-capturing scheme
δ_{ij}	Kronecker delta
Subscript	
i, j, k, m	Index notation
res	Resolved-scale
t	Subgrid-scale
0	Stationary (total) condition
st	Stoichiometric condition
rep	Representative value
Superscript	
$\prime$	Root-mean-square (fluctuations)
$\prime\prime$	Residual

I. Introduction

High-speed propulsion systems, such as (sc)ramjet, have been considered for their relevance to long-range strike and access to orbit. The key advantage of these air-breathing propulsion systems, as compared to conventional rocket engines, is their reduced payload-cost and higher specific impulse. However, the downside of these systems is the stringent requirement to operate over a wide range of operating conditions, in order to facilitate the transition from a low Mach number takeoff to a high-speed supersonic cruise. For this reason, flight-testings of supersonic air-breathing vehicles are accompanied with prohibitive costs. Consequently, most experimental databases for these propulsion systems have been obtained in ground-test facilities, posing an intricate problem to the accurate representation of high-enthalpy flows in actual supersonic flights. An alternative to this issue is to make use of simulation techniques as a predictive tool for the design of these high-speed air-breathing propulsion systems. While conventional Reynolds-Averaged Navier-Stokes (RANS) models have apparent disadvantages that will limit their applications to mere guidelines for the design of such complex configurations, the large-eddy simulation (LES) methods have promising capabilities to accurately describe key features in the engine. In fact, as elaborated in a thorough review by Fureby,[1] the LES methodology has been successful in simulating many supersonic configurations, including dual-mode combustors[2] and scramjet facilities.[3]

However, as with all other novel technologies, the incorporation of numerical simulations in design procedures for air-breathing propulsion systems first requires comprehensive validation of their accuracies; the University of Virginia's dual-mode scramjet experiments are designed exactly to accomplish this requirement. Propagated by the National Center for Hypersonic Combined-Cycle Propulsion (NCHCCP) program,[4] these scramjet experiments performed at the University of Virginia's Supersonic Combustion Facility have contributed to a unique and extensive set of benchmark data that will greatly benefit numerical model validations. To date, non-intrusive diagnostic techniques that have been implemented include focused Schlieren and stereoscopic particle image velocimetry (SPIV),[5] coherent anti-Stokes Raman spectroscopy (CARS),[6] and planar laser induced fluorescence (PLIF),[7] providing measurements of density gradient, velocity fields, hydroxyl radical concentration, temperature, and species mole-fractions. In addition, a numerical study that utilized a hybrid LES/RANS method has also been conducted by Fulton et al.,[8] presenting a preliminary examination of the predictive capabilities of CFD techniques.

The objective of the current study is to evaluate the performance of the steady flamelet/progress variable (F/PV) combustion model[9,10] in the context of the operating point "A" of the University of Virginia's (UV "A") dual-mode scramjet experiments. Similar to other flamelet-based models, the fundamental concept of the F/PV approach is a mapping between all detailed thermochemical quanities and a lower-dimensional manifold, parameterized by two scalars, namely the the mixture-fraction, Z, and the reaction progress variable, C. The advantages of the F/PV model include the precomputation and pretabulation of the thermochemical state-space prior to the simulation, the consideration of turbulence/chemistry interaction using a presumed probability-density function approach, and the consideration of detailed reaction chemistry of arbitrary complexity. However, before we can fully utilize these advantages, it is crucial to first assess the applicability of the F/PV model in high-speed combustion regimes, which are affected by complex aerothermodynamic phenomena. For example, non-linear interactions between turbulence and combustion, unsteady shock waves, scale-separation due to mixed regions of subsonic and supersonic flows, laminar-

turbulent transition, and real gas effects are some challenging yet common features that prevail in the UV "A" scramjet configuration. With the results of this work, we can confidently judge if the benefits of the F/PV formulation will come at the expense of accuracy in representing high-speed reacting flows. Furthermore, this case will serve as the compressible supplement to previous work[11] that analyzes the flamelet-formulation in a low Mach number jet in crossflow configuration. The UV "A"-configuration, the computational setups, such as boundary conditions and model closures, and the shock-detecting scheme that were considered in the present investigation are summarized in the next section. Instantaneous results that compare the performance of different shock-detecting scheme are presented in Sec. III, and the paper finishes with conclusions and plans for future works.

II. Computational Setup

In the following, the setups that constitute the LES computations of the UV "A" scramjet configuration are presented. This discussion begins by presenting the LES-relevant Favre-filtered governing equations; model closures that have been applied to the unclosed terms in these filtered equations are also explained. In Sec. II.B, the geometry and operating conditions of the scramjet configuration and their corresponding numerical treatments are described. A detail discussion of the shock-capturing method and the choice of scalar transport equations is provided in Sec. II.C.

II.A. Governing Equations and Numerical Models

The UV "A" scramjet configuration operates in the supersonic scram-mode. As a result, the flow throughout the combustor-extender section will be predominantly supersonic. Therefore, the appropriate set of governing equations for this analysis corresponds to the compressible Navier-Stokes formulation, which will be filtered for implementations in LES. Noting the convention that Reynolds-filtered and Favre-filtered variables are denoted by $\overline{(\cdot)}$ and $\widetilde{(\cdot)}$, respectively, the relevant transport equations, in conservative form, are:

$$\frac{\partial \overline{\rho}}{\partial t} + \frac{\partial \overline{\rho}\widetilde{u_j}}{\partial x_j} = 0 \,, \tag{1a}$$

$$\frac{\partial \overline{\rho}\widetilde{u_i}}{\partial t} + \frac{\partial \overline{\rho}\widetilde{u_i}\widetilde{u_j}}{\partial x_j} + \frac{\partial \overline{p}}{\partial x_i} = \frac{\partial}{\partial x_j}\left[(\widetilde{\mu}+\mu_t)\left(\frac{\partial \widetilde{u_i}}{\partial x_j} + \frac{\partial \widetilde{u_j}}{\partial x_i} - \frac{2}{3}\delta_{ij}\frac{\partial \widetilde{u_k}}{\partial x_k}\right) - \frac{2}{3}\overline{\rho}k_t\delta_{ij}\right] \,, \tag{1b}$$

$$\frac{\partial \overline{\rho}\widetilde{Z}}{\partial t} + \frac{\partial \overline{\rho}\widetilde{u_j}\widetilde{Z}}{\partial x_j} = \frac{\partial}{\partial x_j}\left[\left(\overline{\rho}\widetilde{D} + \frac{\mu_t}{\mathrm{Sc}_t}\right)\frac{\partial \widetilde{Z}}{\partial x_j}\right] \,, \tag{1c}$$

$$\frac{\partial \overline{\rho}\widetilde{Z''^2}}{\partial t} + \frac{\partial \overline{\rho}\widetilde{u_j}\widetilde{Z''^2}}{\partial x_j} = \frac{\partial}{\partial x_j}\left[\left(\overline{\rho}\widetilde{D} + \frac{\mu_t}{\mathrm{Sc}_t}\right)\frac{\partial \widetilde{Z''^2}}{\partial x_j}\right] - \left[2\overline{\rho}\frac{\mu_t}{\mathrm{Sc}_t}\left(\frac{\partial \widetilde{Z}}{\partial x_j}\right)^2 - 2\overline{\rho}\widetilde{D}\left(\frac{\partial \widetilde{Z'}}{\partial x_j}\right)^2\right] \,, \tag{1d}$$

$$\frac{\partial \overline{\rho}\widetilde{C}}{\partial t} + \frac{\partial \overline{\rho}\widetilde{u_j}\widetilde{C}}{\partial x_j} = \frac{\partial}{\partial x_j}\left[\left(\overline{\rho}\widetilde{D} + \frac{\mu_t}{\mathrm{Sc}_t}\right)\frac{\partial \widetilde{C}}{\partial x_j}\right] + \widetilde{\dot{\omega}_C} \,, \tag{1e}$$

$$\frac{\partial \overline{\rho}\widetilde{E}}{\partial t} + \frac{\partial \overline{\rho}\widetilde{u_j}\widetilde{E}}{\partial x_j} = \frac{\partial}{\partial x_j}\left[\left(\frac{\widetilde{\lambda}}{c_p} + \frac{\mu_t}{\mathrm{Pr}_t}\right)\frac{\partial \widetilde{h}}{\partial x_j}\right] + \frac{\partial}{\partial x_j}\left[-\widetilde{u_j}\overline{p} + \widetilde{u_i}\overline{\tau_{ij}}\right] \,, \tag{1f}$$

where $\widetilde{Z''^2} = \widetilde{Z^2} - \widetilde{Z}^2$ is the mixture-fraction variance. The terms $k_t = 0.5\left(\widetilde{u_i^2} - \widetilde{u_i}^2\right)$ and $2\overline{\rho}\widetilde{D}(\widetilde{\nabla Z'})^2$ are unclosed, and are modeled using the Vreman eddy-viscosity subgrid-scale model[12] and spectral argument,[13] respectively. These models are mathematically expressed as:

$$k_t = \nu_t \left|(a_{ij} + a_{ji})\right| \,, \tag{2a}$$

$$\text{with} \quad \nu_t = \mathcal{C}_\nu\sqrt{\frac{B_\beta}{\alpha_{ij}^2}} \,, \quad \alpha_{ij} = \frac{\partial \widetilde{u_j}}{\partial x_i} \,, \quad \beta_{ij} = \Delta_m^2\alpha_{mi}\alpha_{mj} \,, \quad B_\beta = \frac{1}{2}\sum_{j=1}^{3}\sum_{i=1}^{3}\left(\beta_{ii}\beta_{jj} - \beta_{ij}^2\right) \,,$$

$$2\overline{\rho}\widetilde{D}\left(\widetilde{\frac{\partial Z'}{\partial x_j}}\right)^2 = \overline{\rho}\mathcal{C}_{\widetilde{Q}}\widetilde{Z''^2}\left(\frac{\mu_t}{\mathrm{Sc}_t\Delta^2}\right) \,, \tag{2b}$$

where $\mathcal{C}_\nu$ and $\mathcal{C}_{\widetilde{Q}}$ are model constants set to 0.07 and 40, respectively. The value of the initial chosen model constant corresponds to the maximum theoretical magnitude of eddy viscosity in homogeneous isotropic turbulence, while that of the latter assumes a sufficiently high Reynolds number.

In the present work, the combustion phenomena is modeled by the steady flamelet/progress variable (F/PV) approach,[9,10] with the reaction chemistry represented by a detailed hydrogen-air mechanism consisting of nine species and 19 elementary reactions.[14]

II.B. Geometry, Computational Domain, and Operating Conditions

The geometry and boundary-conditions of the computational domain are shown in Fig. 1. It should be noted, from Fig. 1(a), that this domain covers only part of the entire UV "A" scramjet configuration, namely the isolator, combustor, and extender sections, and excludes the upstream Mach 2 converging-diverging nozzle. Instead, as can be seen in Fig. 1(b), a uniform flow of air consisting of only streamwise velocity component of 1035 m/s (corresponding to a Mach 2 flow based on the static thermodynamic state of $p = 38$ kPa and $T = 667$ K) is imposed at the inflow plane. The fuel-injection is described by a mean uniform flow of pure hydrogen with both streamwise and wall-normal velocity components of 1770 m/s and -220 m/s, respectively, corresponding to a Mach 1.7 condition based on static pressure and temperature of 94 kPa and 190 K, respectively. Artificially generated fluctuations are introduced to the mean fuel-flow to induce the turbulent flow dynamics of the fuel-jet. The global equivalence-ratio that corresponds to these inflow conditions is 0.17, indicating a fuel-lean combustion regime. All walls that envelope the computational domain are prescribed with a no-slip condition and have constant wall-temperature of $T = 600$ K in the non-reacting simulation. In the combusting case, the portion of the top wall and the ramp face, which are highlighted in red in Fig. 1(a), have another isothermal condition of $T = 1000$ K. The marked walls and increased wall-temperature are introduced to approximate the effect of the zirconia insulation applied at these regions in the experiment. The outflow plane is assigned with characteristic boundary-conditions of stationary thermodynamic states, $p_0 = 100$ kPa and $T_0 = 1200$ K.

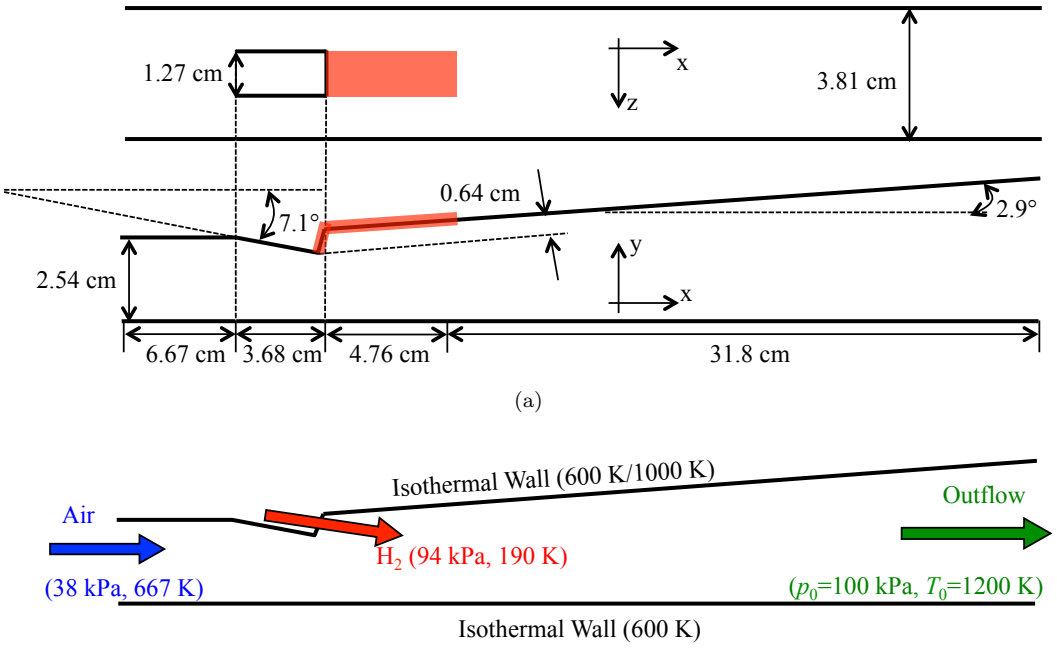

Figure 1. Schematic illustration of the (a) geometry and (b) boundary-conditions of the UV "A" scramjet configuration. As indicated by the various arrows, the general direction of the bulk flow is from left to right.

In addition to the boundary conditions for the hydrodynamic and thermodynamic variables, boundary conditions for all transported scalars are also integral part of the simulation. In this regard, all transported scalars enter the domain with a uniform profile of a certain prescribed value. Specifically, the values of $(\widetilde{Z}, \widetilde{Z''^2}, \widetilde{C})$ are $(0,0,0)$, $(1,0,0)$, and $(0,0,0)$ at the inflow plane, fuel-injection port, and outflow plane,

respectively.

Based on the given operating conditions, a chemistry library was pretabulated using the FlameMaster-code,[15] assuming unity Lewis number for all species. This assumption is reasonable because the transport of species is expected to be dominated by the strong turbulence present in the flow. The current chemistry library is represented by the "S"-shaped curve shown in Fig. 2, which depicts the state space projection of unconvolved temperature and scalar dissipation rate conditioned on stoichiometric mixture-fraction, $Z_{\rm st} = 0.0285$.

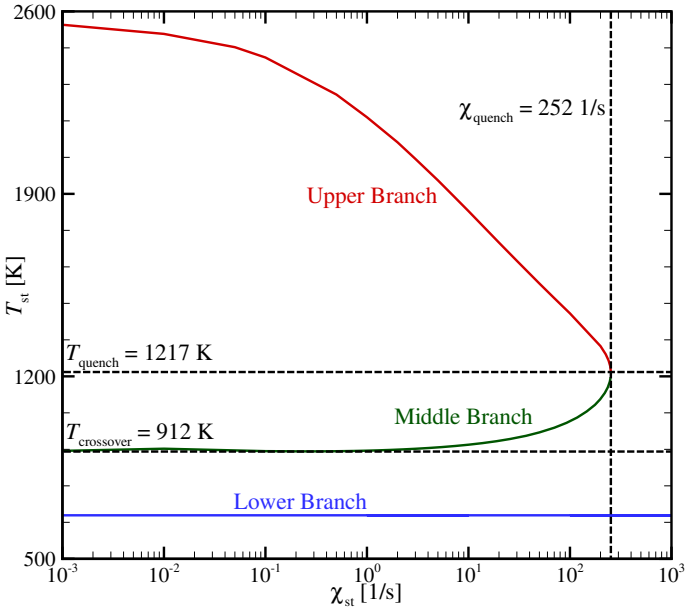

Figure 2. "S"-shaped curve corresponding to the UV "A" scramjet configuration and hydrogen-air mechanism due to Burke *et al.*;[14] stoichiometric mixture-fraction is $Z_{\rm st} = 0.0285$.

From the "S"-shaped curve, we can see that the unstable middle branch is almost horizontal and levels at approximately $T = 912$ K, which is the crossover temperature as pointed out by Hewson & Kerstein.[16] The flatness of the middle branch rules out classical flamelet ignition theory, which requires that the local scalar dissipation rate be lower than a certain critical ignition value in order for self-ignition to occur. Therefore, reactions in our simulation were triggered by artificially rising the progress variable $\widetilde{C}$ to its maximum value. In order to aid in the development of the flame, the early reacting computations are also performed with only the stable upper branch of the "S"-shaped curve, thereby limiting the access of the chemistry library to just the unquenched flame solutions. The eventual transition to the full chemistry library was implemented once the flame stabilized. It is noted that such procedure, while unphysical, is a common strategy in flamelet-based solvers to initiate a flame when auto-ignition is not a dominant flame ignition mechanism.

Currently, the computational domain is discretized by a mixed hexagonal-prism mesh, which consists of approximately 10M control-volumes. The ratio of the unstructured elements (prism) relative to the structured components (hexagonal) is 1.2%, indicating that the computational domain is still largely regular. In order to account for the high shear regions due to mixing of the fuel and the inflow air, the mesh has been statically adapted to have a higher grid density within the volume between the fuel-injection face on the ramp and its projection onto the outflow plane.

Computations of the non-reacting case have been performed on 960 cores of the IBM iDataPlex system Haise at the Navy DoD Supercomputing Resource Center (DSRC), while that of the reacting case are done using 640 cores of the Cray XE6 system Garnet at the U.S. Army Engineer Research and Development Center (ERDC). The computational cost is approximately 13,000 and 10,000 CPU-hours for one characteristic flow-through time of the non-reacting and reacting simulations, respectively. The flow-through time is defined by the domain length from the fuel-injection port to the outflow plane ($\approx$ 36.6 cm) and the fuel-injection speed ($\approx$ 1780 m/s) and is equal to approximately 0.21 ms in physical units.

II.C. Modifications to the Flow Solver

In this study, all simulations are computed using CHRIS, a massively-parallel compressible reacting computational fluid dynamics (CFD) solver developed by Cascade Technologies. However, due to the complexities of the UV "A" scramjet configuration, some critical modifications were required and are addressed in the following.

First, changes were made to the shock-detecting scheme, which will identify and apply the dissipative essentially non-oscillatory (ENO) method to regions with shocks; the rest of the domain is computed using a non-dissipative central differencing scheme. Initially, the shock-detection was based on two general conditions: (i) overshooting in transported scalars (i.e. $\widetilde{Z}$, $\widetilde{Z''^2}$ and/or $\widetilde{C}$); and (ii) magnitude of gradient of the conserved variables, as stated in Eqs. (1). These criteria can be written as:

$$|\phi| > \alpha_1 \ , \tag{3a}$$

$$\left(\frac{\partial \phi}{\partial x_j}\right)^2 \Delta^2 > \alpha_2^2 \times \phi_{\text{rep}}^2 \ . \tag{3b}$$

It was found, by trial-and-error, that setting both α_1 and α_2 to 0.1 seems to give optimal results in terms of shock-capturing. This can be seen in Fig. 3(a) where the ENO scheme is mostly limited to regions that contain shocks or are highly strained by mixing of the reactants (i.e. red regions).

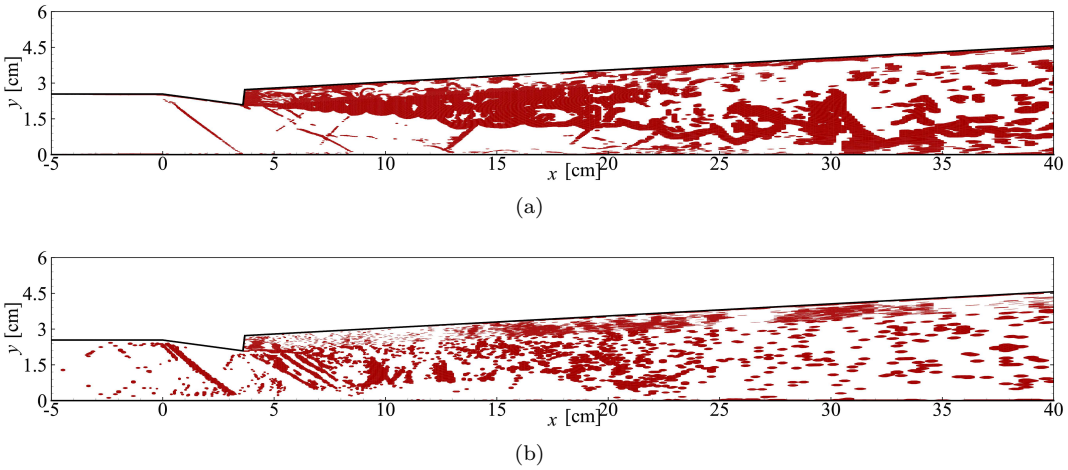

Figure 3. Illustration of the hybrid shock-capturing formulation based on the (a) old and (b) new criteria. Red areas indicate regions where ENO reconstruction has been flagged for implementation. Both figures correspond to the reacting case.

However, as will be further discussed, the previous shock-sensing criteria appear to be too aggressive. Specifically, the localized implementation of the ENO scheme at the high shear region adjacent to the fuel-injection port was found to laminarize the jet stream, delaying the process of jet breakdown and transition to turbulence. In order to circumvent this issue, it is pertinent for the shock-detecting scheme to differentiate between shocks and shear-layers. Our approach to do so is by introducing a new criterion that compares the magnitude of dilatation to that of enstrophy. As pointed out by Ducros *et al.*,[17] dilatation will be negligible relative to enstrophy in most part of a weakly compressible turbulent flow, except in the close vicinities of a shock where dilatation can exceed enstrophy by an order-of-magnitude. The mathematical expression for the dilatation-enstrophy criterion is given by:

$$\frac{\partial \widetilde{u_k}}{\partial x_k} \geq \alpha_3 \sqrt{\widetilde{\omega_k}\widetilde{\omega_k}} \ , \tag{4}$$

where α_3 is set to 0.2, within its typical range of $[0.1,\ 1]$. For the sake of numerical stability, the two initial criteria have to be retained but at a much reduced magnitude, with α_1 and α_2 of 0.05 and 0.5, respectively. The superior performance of the modified shock-detecting scheme over its predecessor is illustrated in Fig. 3(b), where the implementation of the ENO scheme in the high shear region is vastly suppressed, delineating mostly just the shock fronts.

Another modification to CHRIS is the replacement of its default transport equation for $\widetilde{Z^2}$ by that for $\widetilde{Z''^2}$, as shown in Eq. (1d). In contrast to Eq. (1d), previous experience showed that a transport equation for $\widetilde{Z^2}$ is not realizable, allowing for the possibility of physically unrealistic $\widetilde{Z''^2}$ in the solutions.[18] The Eq. (1d), on the other hand, demonstrated that $\widetilde{Z''^2}$ will always be bounded within acceptable deviations from its physical limits.

III. Results

In this section, we will evaluate the differences between the LES results before and after implementing the modifications to CHRIS. The discussion of the reacting solutions will focus on three different planes, namely $z = 0$, $x = 7.493$ cm, and $x = 11.303$ cm. The latter streamwise planes correspond to two of the four planes where experimental CARS measurements of temperature are taken. On the other hand, only results along the mid-plane will be presented for the non-reacting case since it is just conducted to provide a more realistic base flow for the reacting simulations. Figure 4 shows an overview of the evaluated locations along with the outer geometry of the UV "A" scramjet configuration. The planar contour depicts instantaneous temperature profile with stoichiometric mixture-fraction isoline. For convention, we will refer to the lean mixture adjacent to the top wall as the leeward side of the jet, while that next to the inflow air as the windward side of the jet.

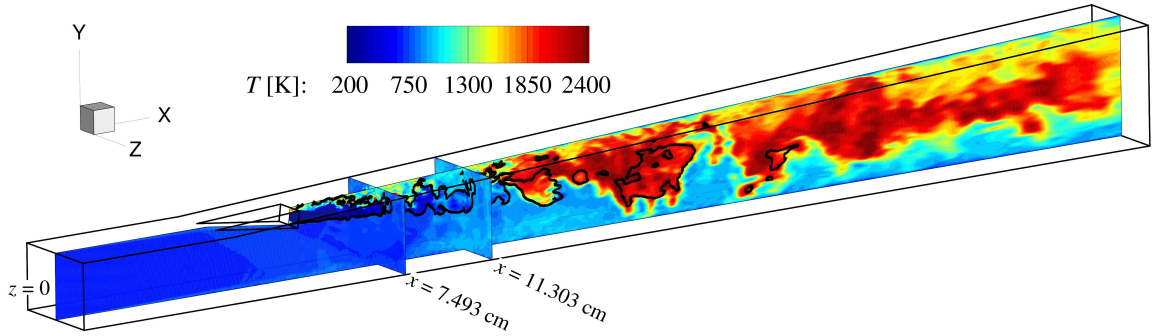

Figure 4. Isometric perspective of the scramjet geometry and the evaluated planes, $z = 0$, $x = 7.493$ cm, and $x = 11.303$ cm. The contour corresponds to the instantaneous temperature distributions and the black lines are the stoichiometric mixture-fraction isolines.

III.A. Prior to Shock-Detecting Scheme Modification

In Sec. II.C, we briefly mentioned that the previous shock-detecting scheme will erroneously laminarize the jet stream. Such artificial laminarization of the jet flow is undesirable because it will delay the jet's laminar-turbulent transition, thereby directly affecting the mixing rate of the fuel and oxidizer streams. As a result, the flame stabilization point may be over-predicted and the entire combustion dynamics may be inaccurate. Even worse, since flameholding relies on a recirculation zone that is located in the leeward region close to the fuel-injection port,[8] this lag in the upstream reaction may lead to an eventual blowoff of the flame.

To demonstrate the unphysical laminarization of the jet, instantaneous temperature, pressure, and streamwise velocity fields of the reacting case using the previous shock-detecting criteria with $\alpha_1 = \alpha_2 = 0.1$ are shown in Fig. 5. The laminar-turbulent transition of the steady fuel jet is most obvious in the temperature field, where we can clearly observe: (i) a relatively homogeneous laminar region adjacent to the fuel-injection point ($3.7 < x < 5$ cm); (ii) a shear-layer instability region ($8 < x < 11$ cm); (iii) an intermediate transition region ($11 < x < 20$ cm); and (iv) a dominantly turbulent region that lasts through the remaining part of the domain ($x > 20$ cm). Comparing the transition region to that of the RANS/LES by Fulton et al.,[8] however, it appears that the current simulation is too diffusive, exhibiting significantly less fine-scale structures than the reference case. This excessive diffusivity is exactly the consequence of the false laminarization of the jet induced by the shock-detecting scheme. Also, the notably higher temperature in the figure than that in Fig. 4 is attributed to the utilization of just the upper stable branch of the "S"-shaped curve. The pressure contour further illustrates that the shock sensor captures much area that does not contain any pressure jump, even though it does correctly identify discontinuities in the pressure field. The streamwise velocity

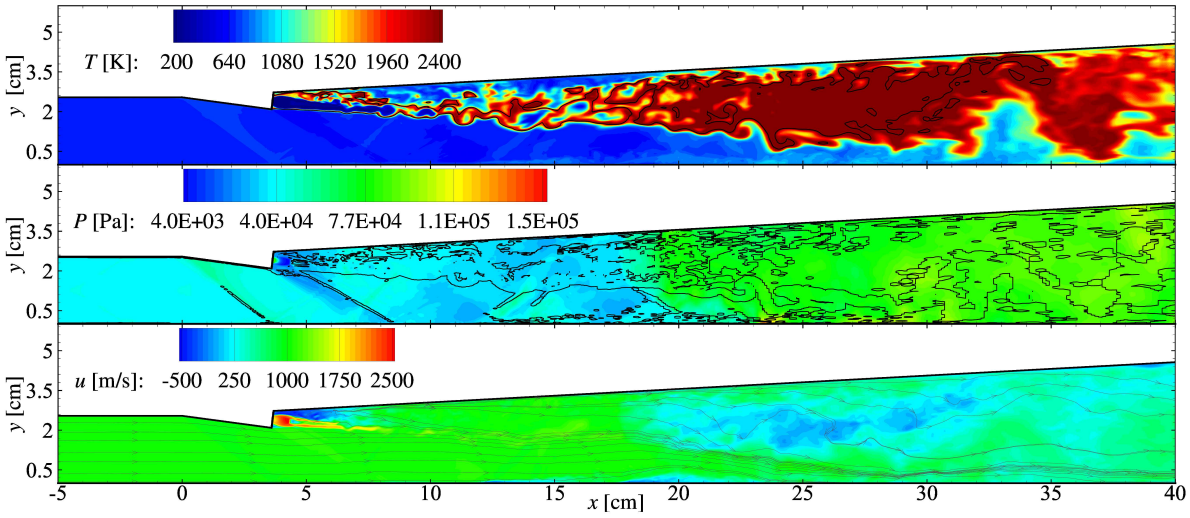

Figure 5. Instantaneous (top) temperature, (middle) pressure, and (bottom) streamwise velocity profile of the reacting case with previous shock-capturing criteria ($\alpha_1 = 0.1$ and $\alpha_2 = 0.1$); the contour lines in these plots correspond to the stoichiometric mixture-fraction, shock sensor flag of one (where ENO method is applied), and two-dimensional flow streamlines, respectively.

component reveals again a laminar region adjacent to the fuel-nozzle, reinforcing the claim that the jet stream is laminarized by the shock-detecting scheme. The plume of reverse flow at the leeward side of the jet is noteworthy, indicating the ability of the flow solver to capture the crucial flame-stabilization mechanism of this configuration.

A clearer depiction of the laminarization of the jet flow can be seen from Fig. 6, where the instantaneous temperature profile along the $x = 7.493$ cm and $x = 11.303$ cm planes exhibit high amount of regularity and approximate symmetry about the $z = 0$ plane. It should be mentioned that these streamwise planes and the mid-plane solution shown in Fig. 5 are extracted from the same instant in time. As illustrated in these streamwise planes, the simulated jet flow has a lower jet spreading rate in x than the experimental CARS measurements.[8] This reduction in the spreading rate may possibly be a consequence of the artificial laminarization of the jet at the upstream locations in the simulations.

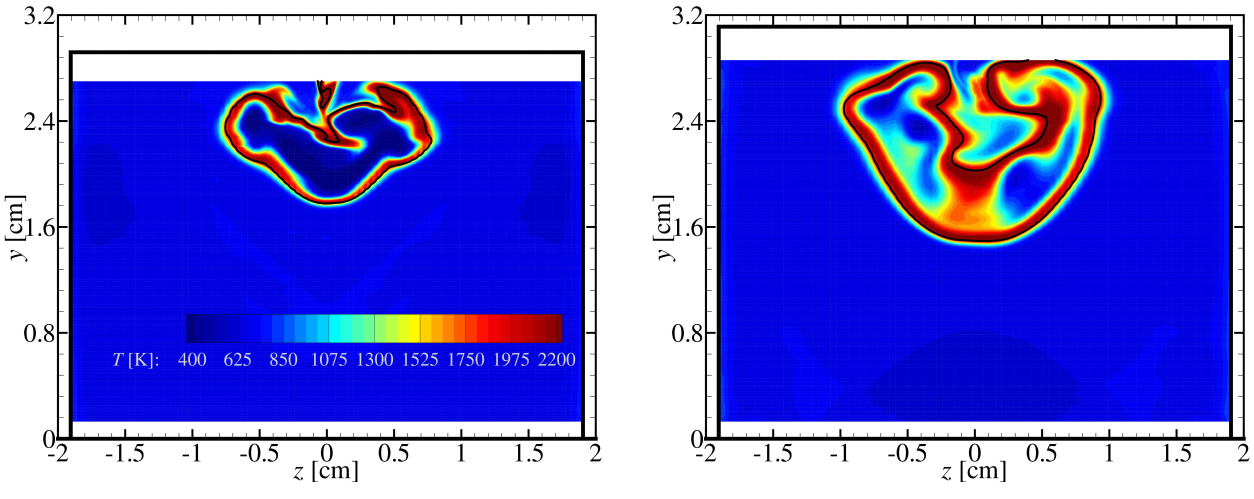

Figure 6. Instantaneous temperature profile at (a) $x = 7.493$ cm and (b) 11.303 cm solved using the previous shock-detecting criteria ($\alpha_1 = 0.1$ and $\alpha_2 = 0.1$). The black isoline denotes the stoichiometric mixture-fraction location. Note that the scaling and range of the results have been adjusted to match that of the experimental CARS measurements shown in Fulton *et al.*[8]

Temperature, pressure, and u-velocity profiles of one snapshot of the non-reacting run are shown in Fig. 7. Since a similar laminar jet flow can be discerned from this temperature contour, we can rule out the possibility that the excessive chemical reaction in the aforementioned reacting case, due to utilization of only the upper stable branch of the "S"-shaped curve, is not the cause of the jet laminarization. From the pressure plot, one can see that the ENO method is applied to a significantly larger area, which does not necessarily contain any shock or shear-layer, than that shown in Fig. 5. This discrepancy in the behavior of the shock-detecting scheme is due to the choice of the shock-sensing parameters of the non-reacting case, $\alpha_1 = 0.1$ and $\alpha_2 = 0.05$, which differ from the observed optimal combination of 0.1 for both α_1 and α_2. We note that a recirculation zone, albeit weaker, is also present in the non-reacting case, demonstrating once again that CHRIS will correctly account for important flow features.

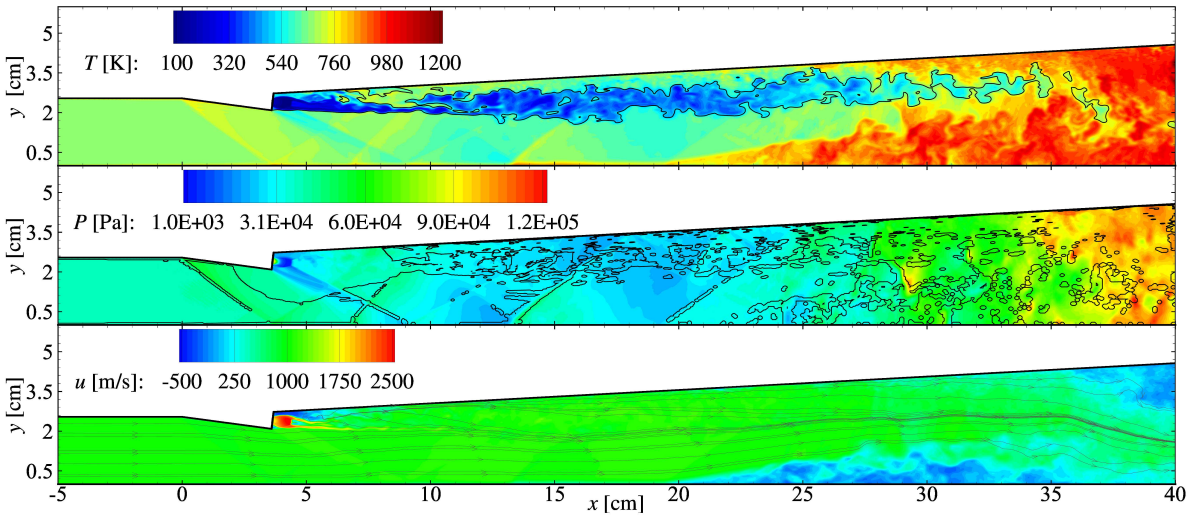

Figure 7. Instantaneous (top) temperature, (middle) pressure, and (bottom) streamwise velocity profile of the non-reacting case with previous shock-capturing criteria ($\alpha_1 = 0.1$ and $\alpha_2 = 0.05$). Plot conventions are the same as that defined by Fig. 5.

III.B. Post Shock-Detecting Scheme Modification

In the following, the results for the reacting run using the new shock-detecting criteria are evaluated. The chosen combination for the shock-sensing parameters is, as described in Sec. II.C, $\alpha_1 = 0.05$, $\alpha_2 = 0.5$, and $\alpha_3 = 0.2$, which seems to be able to capture compressible phenomena effectively without jeopardizing the stability of the numerics. Fig. 8 shows the temperature, pressure, and streamwise velocity profiles resulting from the modification of the shock-detecting scheme. Unlike the temperature plot in Fig. 5, the current temperature contour clearly has more turbulent structures. Sign of a fully-developed turbulent flame occurs as early as $x \approx 13$ cm, and the streamwise penetration of the stoichiometric mixture-fraction is reduced by as much as 50%, indicating a higher mixing rate. The contributing factor that alleviated the jet laminarization issue is the reduction of the influence of the ENO method at the shear-layer vicinities, particularly at the leeward side of the jet, as seen in the pressure plot. This improvement in the prediction of the breakdown of the jet indicates that the new shock-detecting scheme is indeed effective. Similar to the earlier streamwise velocity distributions, the u-profile in Fig. 8 still displays a noticeable flameholding recirculation zone, although the jet stream now exhibits a pulsating-like profile that is unseen previously. Referring to the corresponding streamwise planes $x = 7.493$ cm and $x = 11.303$ cm, as shown in Fig. 9, the temperature profile is obviously more chaotic and no longer preserves a symmetry about the mid-plane. The jet also appears to be more widespread than before, suggesting again that turbulence increases the jet spreading rate in x. It should be mentioned that the results in Fig. 8 are computed using the full chemistry library, in contrast to that shown in Figs. 5 and 6.

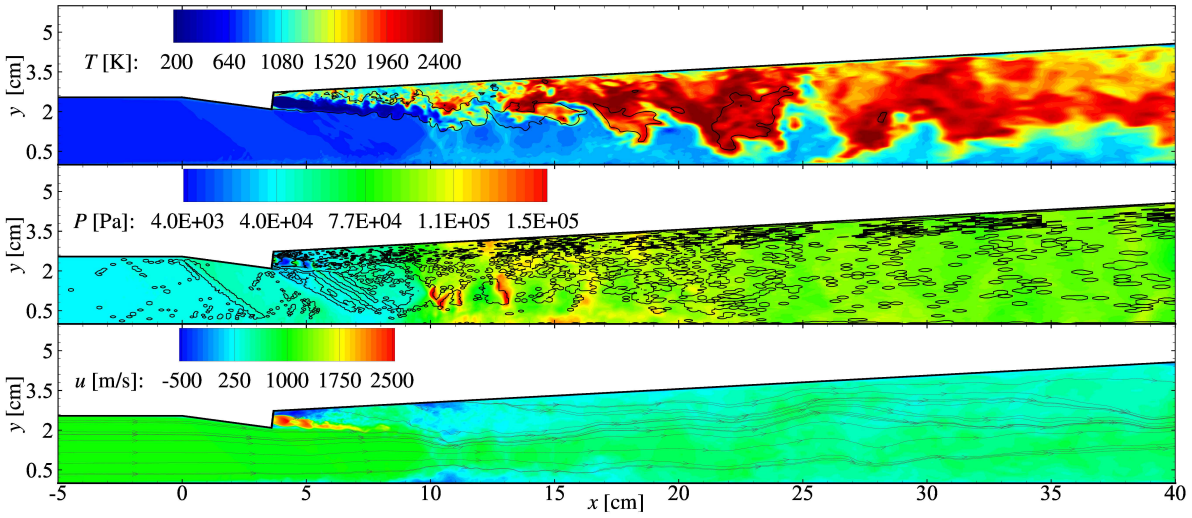

Figure 8. Instantaneous (top) temperature, (middle) pressure, and (bottom) streamwise velocity profile of the reacting case with new shock-capturing criteria ($\alpha_1 = 0.05$, $\alpha_2 = 0.5$, and $\alpha_3 = 0.2$). Plot conventions are the same as that defined by Fig. 5.

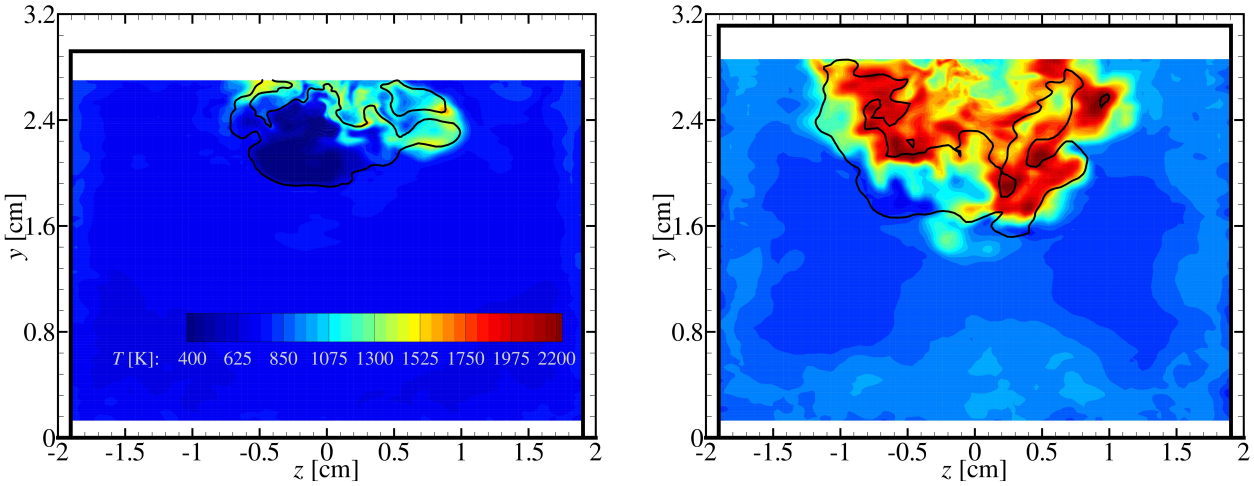

Figure 9. Instantaneous temperature profile at (a) $x = 7.493$ cm and (b) 11.303 cm solved using the new shock-capturing criteria ($\alpha_1 = 0.05$, $\alpha_2 = 0.5$, and $\alpha_3 = 0.2$). Plot conventions are the same as that defined by Fig. 6.

IV. Conclusions

A study that involves the large-eddy simulations of a reacting scramjet is currently being conducted. The geometry of the scramjet of interest corresponds to the "A"-configuration of the University of Virginia's dual-mode scramjet experiments, which is designed to emulate flight conditions at Mach 5 enthalpy. Computations have been performed for both the non-reacting and reacting cases using a massively-parallel compressible reacting solver Chris, which is developed by Cascade Technologies. The current hybrid mesh consists of approximately 10M control-volumes at a ratio of 1.2% between the unstructured and structured elements. Evaluations have shown that: (i) The shock-detecting scheme has significant influence on the development of turbulent structures in the flame, especially in the upstream close-nozzle region. In this regard, the dilatation-enstrophy criterion developed by Ducros *et al.*[17] appears to be an effective and necessary complement to the default shock-capturing criteria in Chris. (ii) The recirculation zone at the leeward side of the jet is present regardless of the case, non-reacting or reacting, and laminarity of the jet stream, suggesting that this region is an inherent feature of the scramjet design. This feature is desirable because the recirculation

zone can provide a flame-anchoring mechanism that sustains combustion in the system.[8] (iii) Transported quantities are in qualitative agreement with a previous numerical study conducted by Fulton *et al.*,[8] which has demonstrated reasonable agreements with its experimental counterpart. (iv) Consistent with Kemenov *et al.*,[18] the transport equation of $\widetilde{Z''^2}$ is found to be much better behaving than that of $\widetilde{Z^2}$.

An outline of the planned work is as follows:

- Converged solutions of the reacting case will be qualitatively and quantitatively compared with the extensive experimental database, which consist of dual-pump coherent anti-Stokes Raman spectroscopy, particle imaging velocimetry, and planar laser-induced fluorescence diagnostics for temperature and species mole-fraction, velocity, and hydroxyl radical concentration.

- Parametric studies on the boundary-conditions will be performed to assess the effects of including/excluding some geometrical features of the scramjet configuration, such as the converging-diverging Mach 2 and conical fuel-injection nozzles, the importance of turbulent fluctuations in the fuel-injection profile, and the appropriateness of the characteristic total outflow boundary-condition.

- Sensitivities of the results to various model closures (e.g. preferential-diffusion phenomenon, and flamelet presumed probability-density-function assumption) will be investigated to identify the potential cause of errors and limitations in the simulations.

Acknowledgments

Financial support through the Air Force Office of Scientific Research under Award No. FA9550-11-1-0031 is gratefully acknowledged.

References

[1]Fureby, C., "LES for supersonic combustion," *18th AIAA/3AF International Space Planes and Hypersonic Systems and Technologies Conference*, AIAA 2012-5979, Tours, France, 2012.

[2]Micka, D. J. and Driscoll, J. F., "Combustion characteristics of a dual-mode scramjet combustor with cavity flameholder," *Proc. Combust. Inst.*, 32, 2009, pp. 2397–2404.

[3]Paull, A., Alesi, H., and Anderson, S., "The HyShot Flight Program and how it was Developed," *AIAA-AAAF 11th Int. Space Planes and Hypersonic Systems and Technologies Conference*, Orleans, France, 2002.

[4]McDaniel, J. C., Chelliah, H., Goyne, C. P., Edwards, J. R., Givi, P., and Cutler, A. D., "US National Center for Hypesonic Combined Cycle Propulsion: An overview," *16th AIAA/DLR/DGLR International Space Planes and Hypersonic Systems and Technologies Conference*, AIAA 2009-7280, Bremen, Germany, 2009.

[5]Rockwell, R. D., J., Goyne, C. P., Rice, B. E., Tatman, B. J., Smith, C., Kouchi, T., McDaniel, J. C., Fulton, J. A., and Edwards, J. R., "Close-collaborative experimental and computational study of a dual-mode scramjet combustor," *50th AIAA Aerospace Sciences Meeting including the New Horizons Forum and Aerospace Exposition*, AIAA 2012-0113, Nashville, TN, 2012.

[6]Cutler, A. D., Magnotti, G., Cantu, L., Gallo, E., Danehy, P. M., Rockwell, R., Goyne, C., and McDaniel, J., "Dual-pump CARS measurements in the Univesity of Virginia's dual-mode scramjet: Configuration "A"," *50th AIAA Aerospace Sciences Meeting including the New Horizons Forum and Aerospace Exposition*, AIAA 2012-0114, Nashville, TN, 2012.

[7]Johansen, C. T., McRae, C. D., Danehy, P. M., Gallo, E., Cantu, L., Magnotti, G., Cutler, A., Rockwell, R. D., Goyne, C. P., and McDaniel, J. C., "OH PLIF Visualization of the UVa Supersonic Combustion Experiment: Configuraton A," *50th AIAA Aerospace Sciences Meeting including the New Horizons Forum and Aerospace Exposition*, AIAA 2012-2887, Nashville, TN, 2012.

[8]Fulton, J. A., Edwards, J. R., Hassan, H. A., Rockwell, R., Goyne, C., McDaniel, J., Smith, C., Cutler, A., Johansen, C., Danehy, P. M., and Kouchi, T., "Large-Eddy/Reynolds-Averaged Navier-Stokes simulations of a dual-mode scramjet combustor," *50th AIAA Aerospace Sciences Meeting including the New Horizons Forum and Aerospace Exposition*, AIAA 2012-0115, Nashville, TN, 2012.

[9]Pierce, C. D. and Moin, P., "Progress-variable approach for large-eddy simulation of non-premixed turbulent combustion," *J. Fluid Mech.*, Vol. 504, 2004, pp. 73–97.

[10]Ihme, M., Cha, C. M., and Pitsch, H., "Prediction of local extinction and re-ignition effects in non-premixed turbulent combustion using a flamelet/progress variable approach," *Proc. Combust. Inst.*, Vol. 30, 2005, pp. 793–800.

[11]Chan, W. L., See, Y. C., Ihme, M., Kolla, H., and Chen, J. H., "Budget analysis and model-assessment of the flamelet-formulation: Application to a reacting jet-in-cross-flow," *Proceedings of the Summer Program*, Center for Turbulence Research, 2012, pp. 397–407.

[12]Vreman, A. W., "An eddy-viscosity subgrid-scale model for turbulent shear flow: Algebraic theory and applications," *Phys. Fluids*, Vol. 16, No. 10, 2004, pp. 3670–3681.

[13]Ihme, M., *Pollutant formation and noise emission in turbulent non-premixed flames*, Ph.D. thesis, Stanford University, 2007.

[14]Burke, M. P., Chaos, M., Ju, Y., Dryer, F. L., and Klippenstein, S. J., "Comprehensive H2/O2 Kinetic Model for High-Pressure Combustion," *Int. J. Chem. Kinet.*, Vol. 44, No. 7, 2011, pp. 444–464.

[15]Pitsch, H., "FlameMaster v3.1: A C++ computer program for 0D combustion and 1D laminar flame calculations," 1998.

[16]Hewson, J. C. and Kerstein, A. R., "Local extinction and reignition in nonpremixed turbulent $CO/H_2/N_2$ jet flames," *Comb. Theory Modelling*, Vol. 174, 2002, pp. 35–66.

[17]Ducros, F., Ferrand, V., Nicoud, F., Weber, C., Darracq, D., Gacherieu, C., and Poinsot, T., "Large-Eddy Simulation of the Shock/Turbulence Interaction," *J. Comp. Phys.*, Vol. 152, 1999, pp. 517–549.

[18]Kemenov, K. A., Wang, H., and Pope, S. B., "Modelling effects of subgrid-scale mixture fraction variance in LES of a piloted diffusion flame," *Comb. Theory Modelling*, Vol. 16, 2012, pp. 611–638.